Radiation Monitoring with Radiosensitive Pure-Silica Core Ultra-Low Loss Optical Fiber

Luca Weninger, *Student Member IEEE*, Adriana Morana, *Member IEEE*, Cosimo Campanella, *Member IEEE*, Jeoffray Vidalot, Emmanuel Marin, Youcef Ouerdane, Aziz Boukenter, Rubén García Alía, *Member IEEE*, and Sylvain Girard, *Senior Member IEEE*

***Abstract* — This article presents a new prospect for radiation detection exploiting the high radiation sensitivity of an ultra-low loss pure-silica core optical fiber (ULL-PSCF). This fiber exhibits very high transient X-ray radiation-induced attenuation (RIA) levels from UV to IR during irradiation while its RIA quickly returns to a low permanent level after irradiation. In this work, the RIA kinetics are investigated exposing the ULL-PSCF to multiple short irradiation runs at different dose rates. A pre-irradiation has been demonstrated to stabilize the response of the optical fiber and to make it even more appealing for radiation detection and monitoring. After this pre-irradiation treatment, the RIAs at 620 nm and 1310 nm in particular exhibit an ON/OFF behavior: the permanent RIA is nearly zero in-between irradiation and the transient RIA quickly increases up to dB/m level when the ULL-PSCF is exposed to X-rays. By varying the fiber length and adapting the interrogation setup, large ranges of doses and dose rates can be detected with this new class of optical fibers.**

***Index Terms*—Radiation detection, optical fibers, RIA, ionizing radiation, sensors, photonics.**

I. INTRODUCTION

RADIATION detectors are a family of sensors that specializes on the detection of ionizing radiation for many different applications. A radiation detector should be able to identify the presence of radiation quickly and reliably, but also to resist to the total ionizing dose (TID) effects without losing its sensing capabilities. Today, many technologies are investigated, from ionizing chambers to photodiodes, from scintillators to optical fibers [1 – 4]. This work focuses on this last category. One of the main mechanisms through which ionizing radiation affects an optical fiber (OF) is called radiation-induced attenuation (RIA). RIA corresponds to an increase of the fiber attenuation. It is caused by the appearance of optical absorption (OA) bands in its transmission windows associated with radiation-induced point defects that are created by ionization or displacement damages within the pure or doped amorphous silica glasses of the OF core and cladding. The structures of these defects and their optical properties depend on the fiber characteristics (*composition, fabrication process, etc*.) [5 – 7]. Furthermore, each defect type can be generated through one or several mechanisms with various efficiencies and will also present its own stability against external stimuli, such as temperature or injected light power. Indeed, at the basis of the measured growth and decay RIA kinetics lies the competition between the generation of new defects and their thermal- or photo-bleaching (PB) [8 – 13]. RIA has been studied over the years on different OFs with the objective to make them either more radiation-hard or more radiation-sensitive, depending on the application needs [5,14]. The main parameter used to classify the OF radiation response is its core and cladding composition. In the literature, pure-silica core (PSC)/F-doped cladding fibers are considered among the most radiation-resistant fibers (together with F-doped OFs) for steady state environments [5,15 – 18]. Recently, a new generation of ultra-low loss pure-silica core optical fibers (ULL-PSCFs), such as the Corning Vascade EX1000, has shown very high and unexpected radiation sensitivity [8,19 – 21]. These Telecom-grade optical fibers implement new fabrication processes to further improve light-guiding capabilities, bringing their 1550 nm intrinsic attenuation down to 0.16 dB/km [19]. In particular, the Vascade OF was shown to be very radiation sensitive in the infrared (IR), even more than the radiation-sensitive P-doped fibers already in use in dosimetry applications, under certain irradiation conditions [22 – 25]. Furthermore, this optical fiber showed an extremely fast recovery kinetics in the IR just after the irradiation: the RIA quickly returns to a low permanent RIA level, almost recovering completely the observed transient RIA [21]. This is a very different feature compared to today used radiosensitive phosphosilicate or aluminosilicate optical fibers that are characterized by no or very limited recovery at these wavelengths [22 – 25]. As the main actors for these transient losses are metastable defects, most of the transient losses are expected to anneal once the irradiation is over, which explains the observed strong recovery. In recent studies, the IR-RIA levels and kinetics of this fiber were also demonstrated to strongly depend on the dose rate and on the injected light power, since this latter can favor a light-assisted recombination phenomenon of the defects, the photo-bleaching [8]. The comparison at different light powers proposed in [8] highlights

Paper submitted for review the 29th September 2023. L. Weninger, A. Morana, C. Campanella, J, Vidalot, E. Marin, Y. Ouerdane, A. Boukenter and S. Girard are with Lab. Hubert Curien, Université Jean Monnet, 42000 Saint-Étienne, France. (e-mail: luca.weninger@univ-st-etienne.fr)

S. Girard is also with Institut Universitaire de France (IUF) Ministère de l'Enseignement Supérieur et de la Recherche sis 1 rue Descartes 75005 Paris, France

Rubén García Alía is with CERN, CH-1211 Genève, Switzerland.
The results presented in this paper have been obtained in the framework of the EU project RADNEXT, receiving funding from the European Union's Horizon 2020 research and innovation programme, Grant Agreement no. 101008126.

the complex RIA dose, dose rate and PB dependence for such fiber. The dependence on the injected light power introduces an interesting tuning possibility for the implementation of this OF as a radiation detector. And while the dose rate dependence of this OF is usually seen as an unwelcome feature which makes it unfit for precise dose sensing, the combination of high sensitivity and strong recovery can become the strong points of a radiation detector, a dose rate meter or a beam loss monitoring system. If confirmed, these two characteristics introduce the advantage of a sensing solution capable of withstanding very large cumulated doses without losing its detection capabilities. This can be a first big advantage of a OF-based detector like this, as semiconductor sensors are also reusable, but suffer from a gradual loss of sensitivity caused by radiation induced damages [26], while P-doped OFs have a linear response only below 1 kGy [5,24]. Other advantages of this solution are the lightness, small size, flexibility and resistance to electromagnetic noise intrinsic of OF-based solutions [27]. Another point in favor of fiber-based sensors is the easiness of implementation as remote solutions, since the associated readout electronics do not need to be exposed to radiations, and the link between the sample and interrogators can be composed of commercially available rad-hard fibers. Last but not least is the tunability of the detector sensitivity by playing with the fiber profile of use: light power, wavelength, type of detector and fiber length. This tunability can also be the main point in favor of a RIA-based solution with this OF when compared with systems based on radiation-induced emission (RIE), as these are the most common choice for fiber-based dose rate sensors [28]. Another advantage of a RIA detector is the possibility of working at telecom wavelengths, opening the way to exploit reflectometry techniques to achieve distributed radiation detection solutions, as it was already demonstrated, e.g. in [22], with a P-doped fiber.

In this paper, we investigate the suitability of this ULL-PSCF to act as a radiation detector by studying its spectral RIA response under irradiation at different dose rates under two different irradiation sequences, measuring both transient (during irradiation) and permanent (after irradiation) RIA levels on both pristine samples and samples that were pre-irradiated at 1 and 2 MGy. In particular, our goal, in the framework of WP5 of the RADNEXT project [29], was to identify the most interesting wavelengths, the capability of our setup to detect a large dose rate range, the dependence of the RIA response against the dose rate and the TID.

II. MEASUREMENT SETUP

A. Optical fibers under test

The investigated optical fiber is an ULL pure-silica core and fluorine-doped cladding single-mode optical fiber, the Vascade EX1000 by Corning. It has an attenuation of 0.16 dB/km at 1550 nm. The spectral characteristics of this fiber, together with the energy-dispersive X-ray (EDX) spectroscopy measurements of its chemical elements and their radial distribution were presented in [19].

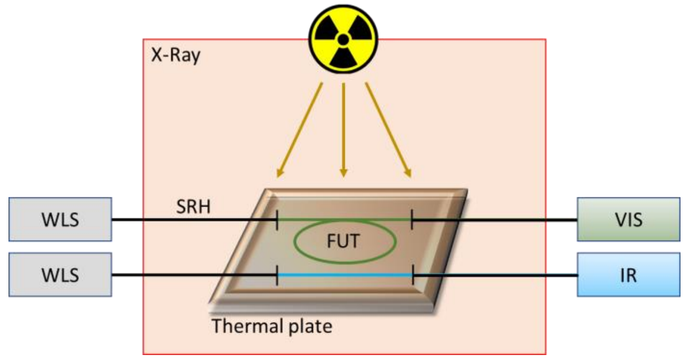

Fig. 1. Dual-channel RIA measurement setup. Each White Light Source (WLS) injects a signal into the transport Super Rad-Hard (SRH) fiber, which passes through our Fibers Under Test (FUT) and another SRH fiber to end in either the Infrared (IR) or Visible (VIS) spectrometer. The FUTs are enclosed in a thermal plate, which is, in turn, placed inside our irradiator.

B. Spectral RIA measuring setup

A spectral analysis gives information about the wavelengths at which the RIA response is the most interesting in terms of radiation sensitivity and compatibility with available interrogation systems. RIA spectra have been obtained through the dual channel setup shown in Fig. 1. Each of the two channels is composed of a white light source (WLS), with a light power of a few µW to minimize PB effect and maximize the induced losses, two single mode super rad-hard (SRH) F-doped transport OFs and one spectrometer, working in the visible (VIS) range (200 – 975 nm) or in the infrared (IR) range (900 – 2140 nm). The previous studies [8,19 – 21] allowed to choose a sample length of ~33 cm for the measurements in the visible and ~24 cm for the measurements in the IR, in order to fully exploit the setup dynamic range in the whole spectral domain for the investigated dose rates. It should be noted that, for the detection of very low radiation dose or dose rates, this length could be increased up to kilometer range thanks to the low initial losses of this fiber. The two fibers under test (FUTs) were arranged in a monolayer spiral inside the LabHX X-ray machine at Lab. Hubert Curien in Saint-Etienne (France), that is equipped with an X-ray tube working at 100 kV, with a tungsten target, which results in an average photon energy-fluence of 40 keV [30]. A thermal plate was used to maintain the sample temperature of all measurements at 22° C. All doses are expressed in Gy(SiO_2).

C. Irradiation procedure

The Vascade response was investigated using the two stepped irradiation profiles illustrated in Fig. 2 and 3. The dose rate was varied by adjusting the X-ray tube current, without changing the distance between the tube and the sample under test. The irradiation sequence in Fig. 2 is composed of a cycle of 5 short runs at increasing dose rates: 0.037, 0.233, 0.465, 4.65 and 14 Gy/s. Each run lasted 5 min, so the accumulated doses for each step were respectively 11.1, 69.9, 139.5, 1395 and 4200 Gy. A 20 min recovery time is considered between two consecutive runs. Then, after 60 min of recovery the whole cycle is repeated but in reverse order.

This article has been accepted for publication in IEEE Transactions on Nuclear Science. This is the author's version which has not been fully edited and content may change prior to final publication. Citation information: DOI 10.1109/TNS.2024.3380999

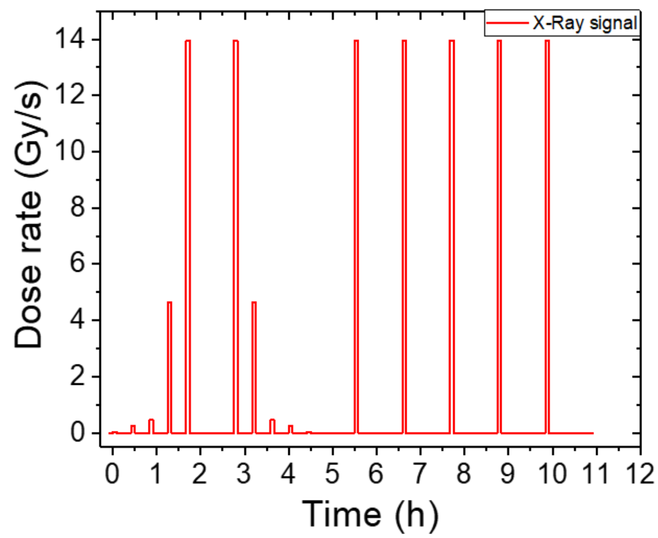

Fig. 2. Ideal interrogation kinetic "5min" over time. At each dose rate, the irradiation was maintained for 5 minutes, while the recovery between steps lasted 20 minutes for the first 5 steps, then 60 minutes before another cycle of 5 steps separated by 20-min pauses and another 5 identical steps each separated by 60 minutes.

Finally, 5 expositions at the highest dose rate (14 Gy/s), each of which 5 minutes long and separated by 60 minutes of pause each time, were carried out. After this process ended, the fiber under test had been exposed to a total dose of ~32 kGy. The goal of this irradiation sequence is to evaluate the capability of this fiber to follow quick changes in the irradiation conditions and the possibility to implement it in a reusable radiation detector. It also lets us distinguish between the growth in permanent losses, observable when no irradiation is present, and transient losses, present only under irradiation. In this paper, this procedure will be referred to as "5min".

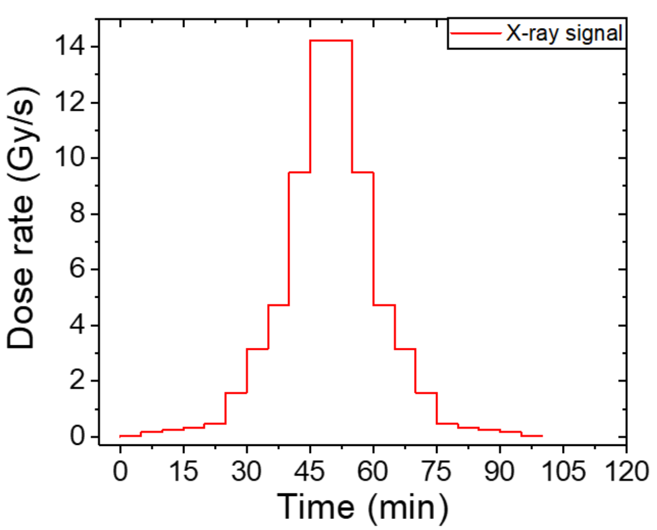

Fig. 3. Ideal interrogation kinetics "DRstep" over time. A continuous irradiation where the dose rate is varied each 5 minutes over 20 steps in ascending and then descending order.

The irradiation sequence in Fig. 3 has the objective to study the capability of the OF to follow dose rate variations without interruptions in the exposition to ionizing radiation. It is composed of 10 5-min steps at different dose rates (from 0.037, to 14.22 Gy/s) in ascending order, and then repeated in descending order. In this paper, this procedure will be referred to as "DRstep".

D. Effects of pre-irradiation at 1 MGy and 2 MGy

To further investigate the RIA response of the Vascade fiber for a possible implementation as a reusable radiation detector able to provide some dosimetry information, the irradiation procedures of Fig. 2 and 3 were repeated a second time on the same sample after it was irradiated up to 1 MGy (at 17 Gy/s for 17 hours) and then a third time after another MGy of dose was deposited, up to 2 MGy, with the same dose rate. In these two cases, to consider the first irradiation as a pre-treatment, the reference signal used to calculate the RIA is the one acquired just before the start of the new irradiation sequence. All these measurements were repeated 2 times for the sake of reproducibility. The figures on this article show the results of the second time the measurements were repeated.

E. Estimation of T_{on} and T_{off}

To conclude the analysis of the kinetics of the irradiation procedure "5min", we evaluated the time delay response of the fiber to irradiation. To do so, we extracted from the measured RIA kinetics the amount of time that took the signal at the highest dose rate (14 Gy/s, only one dose rate for the sake of clarity) to go from 10% to 90% of the average value of the peak, namely the turn-on time (T_{ON}), and the amount of time the RIA needs to go from 90% to 10% of the average value of the peak, namely the turn-off time (T_{OFF}). This approach allows quantification of the transient response of this OF to intermittent irradiations and highlights the impact of different pre-treatments on it.

III. Results

A. Spectral RIA results

Fig. 4 reports the spectral RIA acquired on the Vascade OF after a 4.2 kGy TID (dose rate being 14 Gy/s) and after 10 minutes from the irradiation end. The UV-visible part of the RIA spectrum, which has been less characterized in literature [21], is composed by a more stable band centered at 620 nm and at least one large OA band peaking in the UV below 350 nm. From Fig. 4a, we can see that the bands in this spectral range recover less than the IR part. Indeed, after 10 minutes of recovery the shape of the band at 620 nm is still recognizable, and its peak amplitude changed from 3.7 dB/m to 3 dB/m. For the band in the UV it is difficult to describe any behavior, as what is observable in our results is only an absorption tail resulting from absorption bands peaking outside of our investigated spectral range. The IR-RIA is composed of a wide radiation induced OA band strongly affecting the 2nd and 3rd telecommunication windows (1.31 and 1.55 µm). The large band has a peak at 1310 nm, where it reaches an RIA value of 12 dB/m after 4.2 kGy, which almost completely recovers after only 10 minutes from the irradiation end at room temperature, down to 1.8 dB/m. Indeed, after irradiation the OA band in the IR quickly returns to a lower permanent level, following a quick

This article has been accepted for publication in IEEE Transactions on Nuclear Science. This is the author's version which has not been fully edited and content may change prior to final publication. Citation information: DOI 10.1109/TNS.2024.3380999

recovery kinetics as shown in the inset of Fig. 4a. For comparison, a P-doped fiber at 1550 nm has a RIA-dose sensitivity of about 4 dB/(km Gy) up to ~500 Gy and then it shows a monotonic sublinear behavior at higher doses. Around 2 kGy, the RIA is 7 dB/m [23]. One of the peculiarities of a P-doped OF is the very low recovery, which make it a very capable dosimeter [24]. The peculiarity of the OA bands composing the IR-RIA is that they first very quickly grow before having a less rapid increase (and in some cases a decrease) after a TID of a few kGy (as visible in the inset of Fig. 4a). This very specific behavior justifies the interest in expanding the study on a pre-irradiated OF at higher doses that could exhibit a simpler dose dependence.

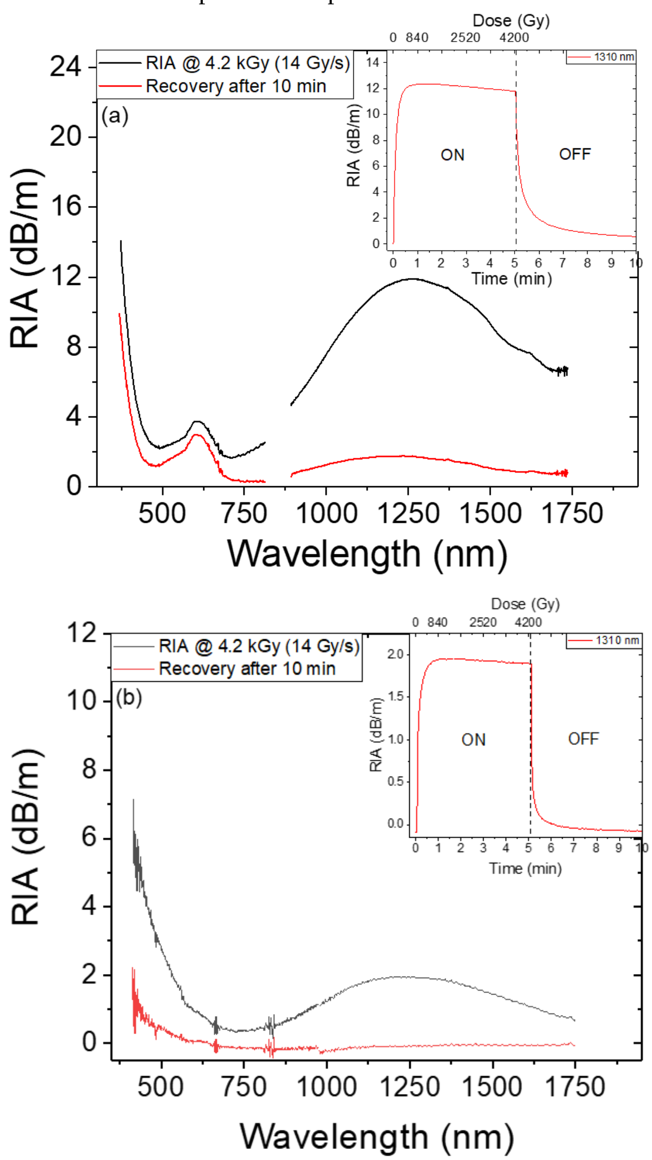

Fig. 4. Spectral X-ray RIA of the Vascade EX1000 OF before (a) and after (b) it was preirradiated at 1 MGy. The black curve reports the spectral RIA measured after 5 minutes irradiation at 14 Gy/s, at a TID of 4.2 kGy. The red curve shows the spectral RIA measured 10 min after irradiation. The inset reports the RIA growth kinetic at 1310 nm for a 5 min irradiation at 14 Gy/s, followed by a recovery phase at room temperature. The dashed line indicates the irradiation end.

Fig. 4b expands this study by presenting the spectral RIA characteristic of an OF that was pre-treated at 1 MGy, again at the peak of a 5-min irradiation at 14 Gy/s (4.2 kGy since the start of the irradiation, shown in the inset) and the recovery after 10 minutes from the irradiation end. It is easy to notice the absence of the OA band at 620 nm which is coherent with its lack of recovery shown in Fig. 4a. This result suggests the room temperature stability of the related defects. After the pre-treatment, the IR-RIA is strongly reduced (~12 dB/m for the pristine sample and ~2 dB/m for the pre-treated sample) and the transient losses recorded during this second irradiation recover completely after 10 minutes. The RIA related to the bands absorbing below 350 nm is reduced by a factor two for the pre-treated sample. It still has a permanent component after a 10 minutes recovery period. In this spectral analysis, it was confirmed that the most interesting wavelengths for this ULL-PSCF are in the infrared domain. Indeed, the band at 620 nm is now integrated inside the permanent attenuation of the fiber after it was irradiated. The large band in the UV-visible below 500 nm could have some interesting behaviors, but only the tail of this large OA band is visible, so additional experiments are needed to discuss about the potential of this spectral region for radiation detection. About the large IR band, as the peak of the band is close to 1310 nm and the kinetics of longer wavelengths are similar to this peak, only less sensitive, we decided to focus our in-depth analysis at 1310 nm, the 2nd telecommunication window.

B. RIA kinetics at 1310 nm: 5min

Fig. 5a presents the RIA kinetics at 1310 nm of the Vascade optical fiber when exposed to the first of the two irradiation sequences presented in Section III.C, called ‘5min’. The black curve reports the kinetics for a pristine fiber. This figure highlights clearly the peculiar behavior of the pristine OF: there is a very quick increase of the IR-RIA during the irradiation and a fast decrease to a low level after the end of each irradiation. In both figures, the times at which the X-ray tube turns ON and OFF are clearly recognizable thanks to the RIA peaks. We can also see that the permanent losses of the pristine fiber grow with the accumulated dose, whereas the transient ones decrease. This decrease in sensitivity while the dose is increasing is also shown in the reduced height of the peaks for the red and blue curves. These two curves represent the results for the samples that were pre-irradiated at 1 and 2 MGy. Since the reference signal over which the RIA is calculated is acquired just before the start of the first irradiation step, at time equals to 0 in the figure, the RIA here reported for the pre-treated samples takes only into account the induced losses caused by this new series of irradiations. This approach highlights the absence of permanent RIA during these irradiation runs and, consequently, the stability of the permanent RIA induced during the pre-treatment at 1 or 2 MGy. The RIA kinetics at this wavelength returns readily close to 0 just after irradiation. So, the main contribution in all of these curves comes from the transient RIA. Their peak values when exposed to the maximum dose rate stabilize around a similar value as the accumulated dose increases. The fluctuations observed in the permanent losses of the red and blue curves can be explained by the short fiber length paired with the decrease in sensitivity induced by the pre-irradiation.

This article has been accepted for publication in IEEE Transactions on Nuclear Science. This is the author's version which has not been fully edited and content may change prior to final publication. Citation information: DOI 10.1109/TNS.2024.3380999

This forced these measurements at the limit of the dynamic range of the used setup. The maximum magnitude of these fluctuations is 0.32 dB/m (red) and 0.38 dB/m (blue), which for a 24 cm fiber translates to a variation of 0.09 dB and 0.08 dB, respectively. A longer fiber length will easily solve this issue, but the peaks at 14 Gy/s of the pristine sample would have been outside of our measurement range. It is worth mentioning that for the pre-irradiated samples, the difference between the average value of the peak and the RIA just before the irradiation is constant across all runs.

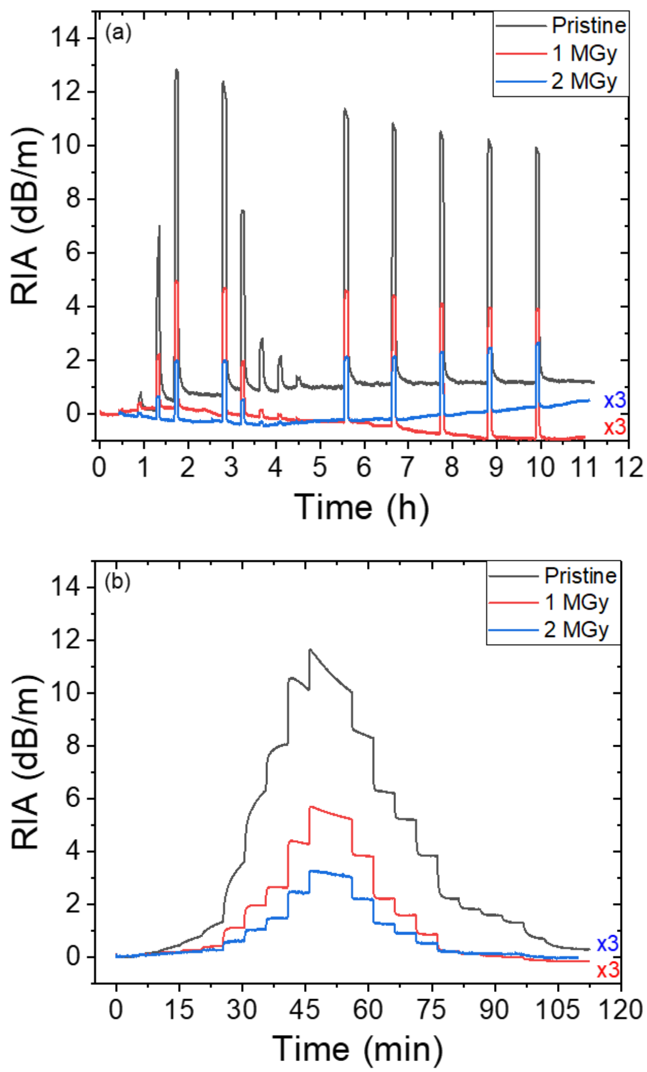

Fig. 5. RIA kinetics at 1310 nm during the two types of irradiation sequences after being irradiated at 3 dose levels. a) Kinetics at 1310 nm of the OF when exposed to the '5min' procedure of Fig. 2. b) Kinetics at 1310 of the Vascade OF when exposed to the 'DRstep' procedure of Fig. 3. In both graphs, the blue and red curves, representing the RIA kinetics after 1 MGy and 2 MGy, have been magnified by a factor three to visually aid the comparison between the curves.

C. T_{ON} and T_{OFF} estimation: 5min

Table I reports the estimated T_{ON} and T_{OFF} for the peaks at the highest dose rate (14.22 Gy/s) of the three curves shown in Fig. 5a. The reported values are the average and the standard deviation of T_{ON} and T_{OFF} calculated across the seven peaks performed at the maximum dose rate during an irradiation sequence. With the pristine sample, it takes about 15 seconds for the RIA to reach 90% of its peak value, before settling toward a slightly lower level. After the irradiation end, it takes about 100 seconds for the RIA to return to less than 10% of its peak value. The T_{ON} value for the pristine fiber is not directly comparable with the values for the pre-irradiated fibers, as the kinetics of the peaks in the first case is composed of an overshoot which then settles towards the final value. This explains the low T_{ON} value, as it was severely underestimated because of the overshoot. With the pre-irradiation, in agreement with the previous results that showed that the fiber is more efficient in monitoring dose rate changes, both T_{ON} and T_{OFF} decrease monotonically with the dose. This is particularly clear in the T_{OFF} values, decreasing from 104 seconds to ~13 seconds, highlighting that the pre-treated fiber is much more responsive to the radiation presence.

TABLE I. TURN ON AND TURN OFF TIME RESULTS AT 14.22 GY/S

Starting dose (MGy)	T_{ON} (s)	T_{OFF} (s)
0	15 ± 7	104 ± 28
1	24 ± 2	23 ± 2
2	15 ± 2	13 ± 2

D. RIA kinetics at 1310 nm: DRstep

The RIA response to the irradiation sequence 'DRstep' is presented in Fig. 5b. With this experiment, it is possible to appreciate this fiber capability to follow the variations in dose rate during a long irradiation. The black curve shows the result for the pristine fiber. The RIA obtained during the ascending steps is higher than during the descending ones. This agrees with the accumulated dose effect of Fig. 5a. The rounded edges are due to a slower response of the RIA observed at low doses, that can also be observed for the '5min' procedure. At the two highest dose rates, the response is similar to the inset of Fig. 4a, where the RIA quickly reaches a maximum and then starts decreasing. After the maximum dose rate is reached (~10 kGy), the OF is able to follow well each step of the decreasing dose rate succession. The pre-irradiated curves show an improvement in the capability of the OF to follow dose rate changes in this experiment too. The RIA response decreased again, from ~12 dB/m at the highest dose rate to ~2 dB/m after 1 MGy and ~1.2 dB/m after 2 MGy. This decrease in sensitivity is accompanied by an increase in the stability of each step and in the response quickness of the RIA, which is coherent with Section III.C.

IV. DISCUSSION

The results presented in Fig. 6 were obtained by averaging the last 3 minutes of RIA at each dose rate step, for the two irradiation procedures. As the experiments were repeated two times, the points in this figure represent the average value and the standard deviation between the two. It is worth mentioning that for most of the points on the graph the error bars are smaller than the symbol size, therefore invisible. The separation of the average RIA values while the dose rate ascends or descends

This article has been accepted for publication in IEEE Transactions on Nuclear Science. This is the author's version which has not been fully edited and content may change prior to final publication. Citation information: DOI 10.1109/TNS.2024.3380999

(empty or full symbols, respectively) has been introduced to highlight the different behavior between the two regimes on the pristine fiber in Fig. 6a. Here it can be seen that the empty symbols are lower than the full ones, which can be traced back to the same build-up behavior discussed about the kinetics of Fig. 5. Looking at this kinetics, one would expect the value during the ascending dose rate phase (empty symbols) to be higher than the descending dose rate one (full symbols), as the maximum values of each peak clearly decreases with the increasing dose. This incoherence is caused by the different shape of the peaks, which are rounder due to the slower response of the fiber when pristine. This implies that calculating the average across the last 3 minutes of a peak will inevitably result in a lower value than the maximum value of the peak.

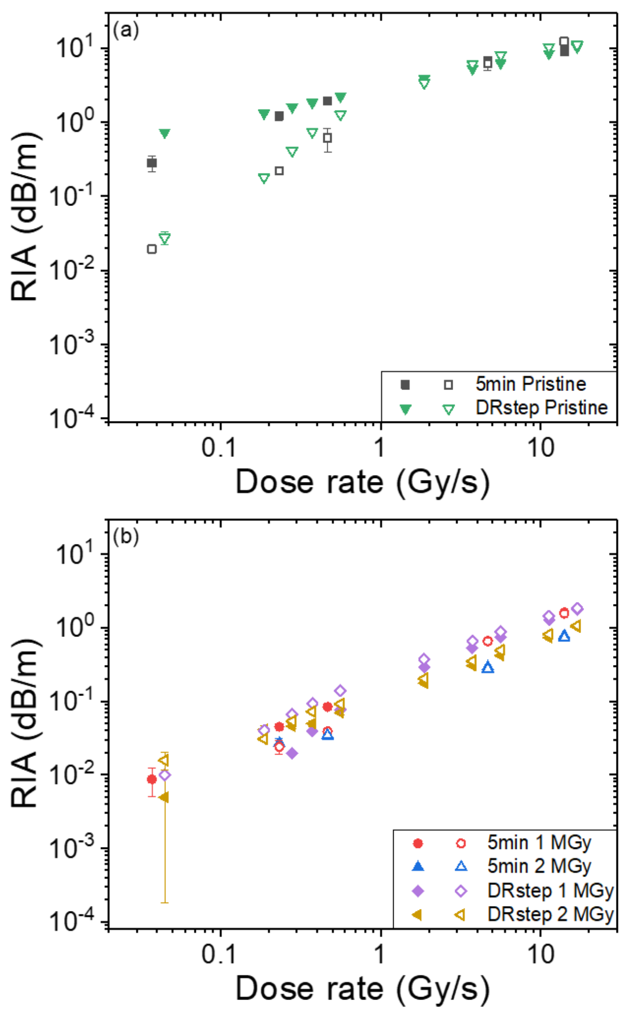

Fig. 6. Average RIA signal per peak at different dose rates, for the pristine (a) and pre-irradiated (b) samples. Each point represents average across two measurements in the same condition. The error bars report the standard deviation calculated between the two measurements (for most of the points they are smaller than the symbol size). The empty points report the RIA values about when the dose rate was increasing, while the full ones show the results for the descending part of the irradiation sequence.

The results shown in Fig. 6b for the pre-irradiated fibers show a decrease in sensitivity but also clear improvement in the linearity of the response. This result is confirmed by the values presented in Table II, which report the slopes and R^2 values for the simple linear regressions that were applied to each data set. The different behavior of the pristine fiber with respect to irradiated ones can be explained by the coexistence during the first irradiation of the generation processes of both stable defects, which will then constitute the permanent losses present after irradiation, and unstable defects, which compose the transient losses following closely the dose rate variations.

TABLE II. LINEAR REGRESSION RESULTS

Irradiation procedure	Dose (MGy)	Slope (dB s m^{-1} Gy^{-1})	Adj. R^2
5min	0	0.8 ± 0.1	0.83584
	1	0.115 ± 0.001	0.99872
	2	0.0548 ± $6x10^{-4}$	0.99841
DRstep	0	1.4 ± 0.2	0.7278
	1	0.134 ± 0.005	0.97026
	2	0.069 ± 0.002	0.97694

Once the stable defects have been generated from their precursors, they will be part of the initial losses of the pre-treated fibers. These will then better follow the dose rate changes, as the largest component of their RIA will be the transient losses, thus the OA contribution of the unstable defects. The pre-treatment is then confirmed to improve the dosimetric capabilities of this optical fiber, as it improves the linearity and the responsiveness of the RIA evolution at 1310 nm to dose rate. The reduction in sensitivity and thus the lower detection capability of a dosimeter like this can be easily compensated with more fiber length, as the results presented in this paper for the IR-RIA were achieved with only 24 cm of fiber. The RIA response to dose rate can also be tuned with the choice of the light source used for the interrogation system, as the PB effect discussed in [8] shows that a stronger injected power can mitigate part of the losses of this optical fiber. The results shown in Fig. 6 and Table II additionally give information about the dose independency of this dosimeter, which is a requirement for a dose rate sensor. At the very least, these results show that the sensitivity decreased only by a factor 2 between 1 and 2 MGy of dose. This means that it is possible to reliably calibrate this optical fiber around a certain dose and define an operating dose range. As the difference in sensitivity is so low, a careful calibration of the fiber could also lead to dose-compensated measurements. This would greatly expand the range of doses a fiber like this could be used in. It is also worth mentioning that all these results were shown at 1310 nm because this wavelength is at the center of the 2nd telecommunication window. The dosimetric capabilities of this fiber at this wavelength can then be easily paired with the great number of interrogation devices and techniques that have been developed over the years for fiber-based communication technologies. Examples are optical time-domain reflectometry (OTDR) or optical frequency-domain reflectometry (OFDR) techniques for distributed RIA measurements [22,31 – 33], or monochromatic interrogators for point RIA measurements [34,35]. If needed, it is also possible to implement interrogators based on the 3rd telecommunication window, at 1550 nm, as the spectral results in Fig. 4 show close RIA kinetics at this wavelength, but with a lower radiation sensitivity.

V. Conclusions

The spectral RIA curves in Fig. 4 show the good compatibility of this OF with telecom-grade interrogation systems, with the highest sensitivity around 1310 nm. At this wavelength, and for the pre-irradiated samples, the transient RIA level faithfully follows the exposition to different dose rates, while the permanent RIA does not change with the absorbed dose. The results of the pre-treatment exhibit a higher linearity of the RIA vs dose rate characteristic ($R^2 > 0.97$) and a quicker response in time to dose rate change. This comes at the cost of a lower sensitivity per unit length, but this can be very easily compensated with a longer sample length. The sensitivity is also tunable by adapting the fiber profile of use as seen in a previous work [8]. The results in this article ultimately show the promise of this ULL-PSCF to serve as the active element of a dose rate monitor, e.g. for beam loss monitoring, thanks to its tunable sensitivity and linear RIA response. The implementation of an optical fiber-based system like this would then bear the advantage of the EM immunity, small dimension and weight intrinsic to optical fibers. The characterized wavelength, 1310 nm, implies the compatibility of the results with many interrogation techniques designed for telecommunications. These systems could then be low cost as built with Telecom-grade optical fibers and interrogators. This also confirms the possibility of achieving, among others, remote sensing and spatially-resolved solutions by combining such optical fiber with reflectometry techniques. To complete the characterization of this optical fiber, the RIA response of this fiber should be investigated at different temperatures, as the presented results were all obtained while keeping the temperature fixed at 22° C. This will be the topic of a future study.

References

[1] K. Wittenburg, “Beam Loss Monitors,” Jun. 2018, doi: 10.48550/ARXIV.2005.06522.

[2] F. Wulf, M. Korfer, W. Goettmann, and H.-J. Grabosch, “Beam loss monitors for FEL using optical fiber,” in *2009 IEEE Nuclear Science Symposium Conference Record (NSS/MIC)*, Orlando, FL: IEEE, Oct. 2009, pp. 1993–1997. doi: 10.1109/NSSMIC.2009.5402133.

[3] G. Spiezia *et al.*, “The LHC Radiation Monitoring System - RadMon,” presented at the 10th International Conference on Large Scale Applications and Radiation Hardness of Semiconductor Detectors, Firenze, Italy, Jul. 2011.

[4] K. Biłko *et al.*, “Radiation environment in the Large Hadron Collider during the 2022 restart and related RHA implications,” *IEEE Trans. Nucl. Sci.*, Early Access, 2024, doi: 10.1109/TNS.2023.3328145.

[5] S. Girard *et al.*, “Overview of radiation induced point defects in silica-based optical fibers,” *Reviews in Physics*, vol. 4, Art. no. 100032, Nov. 2019, doi: 10.1016/j.revip.2019.100032.

[6] S. Girard *et al.*, “Radiation Effects on Silica-Based Optical Fibers: Recent Advances and Future Challenges,” *IEEE Trans. Nucl. Sci.*, vol. 60, no. 3, pp. 2015–2036, Jun. 2013, doi: 10.1109/TNS.2012.2235464.

[7] S. Girard *et al.*, “Recent advances in radiation-hardened fiber-based technologies for space applications,” *J. Opt.*, vol. 20, no. 9, Art. no. 093001, Sep. 2018, doi: 10.1088/2040-8986/aad271.

[8] C. Campanella *et al.*, “Photobleaching Effect on the Radiation-Induced Attenuation of an Ultralow Loss Optical Fiber at Telecommunication Wavelengths,” *Physica Status Solidi (a)*, vol. 219, no. 2, Art. no. 2100518, Jan. 2022, doi: 10.1002/pssa.202100518.

[9] C. Campanella *et al.*, “Influence of Ambient Light on the Radiation-Induced Attenuation of Germanosilicate Optical Fibers in the Visible and Near-Infrared Domains,” *IEEE Trans. Nucl. Sci.*, vol. 70, no. 4, pp. 562–567, Apr. 2023, doi: 10.1109/TNS.2022.3228099.

[10] C. Campanella *et al.*, “Photobleaching Effect on Infrared Radiation-Induced Attenuation of Germanosilicate Optical Fibers at MGy Dose Levels,” *IEEE Trans. Nucl. Sci.*, vol. 68, no. 8, pp. 1688–1693, Aug. 2021, doi: 10.1109/TNS.2021.3068829.

[11] C. Campanella *et al.*, “Combined Temperature and Radiation Effects on Radiation-Sensitive Single-Mode Optical Fibers,” *IEEE Trans. Nucl. Sci.*, vol. 67, no. 7, pp. 1643–1649, Jul. 2020, doi: 10.1109/TNS.2020.2982280.

[12] S. Girard *et al.*, “Combined High Dose and Temperature Radiation Effects on Multimode Silica-Based Optical Fibers,” *IEEE Trans. Nucl. Sci.*, vol. 60, no. 6, pp. 4305–4313, Dec. 2013, doi: 10.1109/TNS.2013.2281832.

[13] A. Morana *et al.*, “Temperature Dependence of Radiation-Induced Attenuation of a Fluorine-Doped Single-Mode Optical Fiber at Infrared Wavelengths,” *IEEE Trans. Nucl. Sci.*, vol. 70, no. 4, pp. 549–555, Apr. 2023, doi: 10.1109/TNS.2023.3239986.

[14] A. L. Tomashuk and K. M. Golant, “Radiation-resistant and radiation-sensitive silica optical fibers,” presented at the Advances in Fiber Optics, E. M. Dianov, Ed., Moscow, Russia, May 2000, Proc. SPIE 4083 . doi: 10.1117/12.385646.

[15] A. L. Tomashuk *et al.*, “Role of Inherent Radiation-Induced Self-Trapped Holes in Pulsed-Radiation Effect on Pure-Silica-Core Optical Fibers,” *J. Lightwave Technol.*, vol. 37, no. 3, pp. 956–963, Feb. 2019, doi: 10.1109/JLT.2018.2884078.

[16] P. F. Kashaykin, A. L. Tomashuk, M. Yu. Salgansky, A. N. Guryanov, and E. M. Dianov, “Anomalies and peculiarities of radiation-induced light absorption in pure silica optical fibers at different temperatures,” *Journal of Applied Physics*, vol. 121, no. 21, Art. no. 213104, Jun. 2017, doi: 10.1063/1.4984601.

[17] T. J. Wijnands, S. K. Hoeffgen, U. Weinand, J. Kuhnhenn, and L. K. De Jonge, “Optical absorption in commercial single mode optical fibres for the LHC machine,” 2007, doi: 10.5170/CERN-2007-007.121.

[18] T. Wijnands, L. K. De Jonge, J. Kuhnhenn, S. K. Hoeffgen, and U. Weinand, “Optical Absorption in Commercial Single Mode Optical Fibers in a High Energy Physics Radiation Field,” *IEEE Trans. Nucl. Sci.*, vol. 55, no. 4, pp. 2216–2222, Aug. 2008, doi: 10.1109/TNS.2008.2001859.

[19] A. Morana *et al.*, “Extreme Radiation Sensitivity of Ultra-Low Loss Pure-Silica-Core Optical Fibers at Low Dose Levels and Infrared Wavelengths,” *Sensors*, vol. 20, no. 24, Art. no. 7254, Dec. 2020, doi: 10.3390/s20247254.

[20] V. De Michele *et al.*, “Pulsed X-Ray Radiation Response of Ultralow Loss Pure-Silica-Core Optical Fibers,” *Physica Status Solidi (a)*, vol. 219, no. 2, Art. no. 2100519, Jan. 2022, doi: 10.1002/pssa.202100519.

[21] S. Girard *et al.*, “Radiation responses of ultra-low loss pure-silica-core optical fibers in the visible to infrared domains,” *Optical Materials: X*, vol. 16, Art. no. 100191, Oct. 2022, doi: 10.1016/j.omx.2022.100191.

[22] D. Di Francesca *et al.*, “Distributed Optical Fiber Radiation Sensing in the Proton Synchrotron Booster at CERN,” *IEEE Trans. Nucl. Sci.*, vol. 65, no. 8, pp. 1639–1644, Aug. 2018, doi: 10.1109/TNS.2018.2818760.

[23] D. Di Francesca *et al.*, “Qualification and Calibration of Single-Mode Phosphosilicate Optical Fiber for Dosimetry at CERN,” *J. Lightwave Technol.*, vol. 37, no. 18, pp. 4643–4649, Sep. 2019, doi: 10.1109/JLT.2019.2915510.

[24] L. Weninger *et al.*, “Calibration in the Visible and Infrared Domains of Multimode Phosphosilicate Optical Fibers for Dosimetry Applications,” *IEEE Trans. Nucl. Sci.*, vol. 70, no. 8, pp. 1908–1916, Aug. 2023, doi: 10.1109/TNS.2023.3252941.

[25] S. Girard, Y. Ouerdane, C. Marcandella, A. Boukenter, S. Quenard, and N. Authier, “Feasibility of radiation dosimetry with phosphorus-doped optical fibers in the ultraviolet and visible domain,” *Journal of Non-Crystalline Solids*, vol. 357, no. 8–9, pp. 1871–1874, Apr. 2011, doi: 10.1016/j.jnoncrysol.2010.11.113.

[26] A. Karmakar, J. Wang, J. Prinzie, V. De Smedt, and P. Leroux, “A Review of Semiconductor Based Ionising Radiation Sensors Used in Harsh Radiation Environments and Their Applications,” *Radiation*, vol. 1, no. 3, pp. 194–217, Aug. 2021, doi: 10.3390/radiation1030018.

[27] J. Zhang, Y. Xiang, C. Wang, Y. Chen, S. C. Tjin, and L. Wei, “Recent Advances in Optical Fiber Enabled Radiation Sensors,”

Sensors, vol. 22, no. 3, Art. no. 1126, Feb. 2022, doi: 10.3390/s22031126.

[28] S. O'Keeffe *et al.*, "A review of recent advances in optical fibre sensors for *in vivo* dosimetry during radiotherapy," *BJR*, vol. 88, no. 1050, Art. no. 20140702, Jun. 2015, doi: 10.1259/bjr.20140702.

[29] R. G. Alía *et al.*, "Heavy Ion Energy Deposition and SEE Intercomparison Within the RADNEXT Irradiation Facility Network," *IEEE Trans. Nucl. Sci.*, vol. 70, no. 8, pp. 1596–1605, Aug. 2023, doi: 10.1109/TNS.2023.3260309.

[30] A. Meyer, D. Lambert, A. Morana, P. Paillet, A. Boukenter, and S. Girard, "Simulation and Optimization of Optical Fiber Irradiation with X-rays at Different Energies," *Radiation*, vol. 3, no. 1, pp. 58–74, Mar. 2023, doi: 10.3390/radiation3010006.

[31] A. Meyer *et al.*, "Toward an Embedded and Distributed Optical Fiber-Based Dosimeter for Space Applications," *IEEE Trans. Nucl. Sci.*, vol. 70, no. 4, pp. 583–589, Apr. 2023, doi: 10.1109/TNS.2022.3226194.

[32] A. V. Faustov *et al.*, "Remote distributed optical fibre dose measuring of high gamma-irradiation with highly sensitive Al- and P-doped fibres," presented at the SPIE Optics + Optoelectronics, F. Baldini, J. Homola, and R. A. Lieberman, Eds., Prague, Czech Republic, May 2013, Art. no. 877404. doi: 10.1117/12.2017331.

[33] A. V. Faustov *et al.*, "Application of phosphate doped fibers for OFDR dosimetry," *Results in Physics*, vol. 6, pp. 86–87, 2016, doi: 10.1016/j.rinp.2016.02.001.

[34] D. Di Francesca *et al.*, "Low radiation dose calibration and theoretical model of an optical fiber dosimeter for the International Space Station," *Appl. Opt.*, vol. 62, no. 16, pp. E43-E50, Jun. 2023, doi: 10.1364/AO.483560.

[35] M. Roche *et al.*, "Solar Particle Event Detection with the LUMINA Optical Fiber Dosimeter aboard the International Space Station," *IEEE Trans. Nucl. Sci.*, Early Access, 2024, doi: 10.1109/TNS.2024.3368137.